

# UAV-Assisted Intelligent Reflecting Surface Symbiotic Radio System

Meng Hua, Luxi Yang, *Senior Member, IEEE*, Qingqing Wu, Cunhua Pan,  
Chunguo Li, *Senior Member, IEEE*, and A. Lee Swindlehurst, *Fellow, IEEE*

## Abstract

This paper investigates a symbiotic unmanned aerial vehicle (UAV)-assisted intelligent reflecting surface (IRS) radio system, where the UAV is leveraged to help the IRS reflect its own signals to the base station (BS), and meanwhile enhance the UAV transmission by passive beamforming at the IRS. First, we consider the problem of maximizing the minimum rate of the IRS by jointly optimizing the UAV trajectory, IRS phase shift matrix, and IRS scheduling, subject to the minimum primary rate requirements of the UAV. We find that conventional relaxation-based methods cannot solve this mixed integer non-convex problem since the minimum primary rate requirements may not be satisfied by the binary reconstruction operation. To address this issue, we first transform the binary constraints into an equivalent series of equality constraints. Then, a penalty-based algorithm is proposed to obtain a high-quality suboptimal solution. Second, we consider the weighted sum-rate maximization problem among all IRS. Although the proposed penalty-based algorithm can also be applied to this problem, it incurs high computational complexity. To reduce its complexity, we first relax the binary variables into continuous variables, and then propose an alternating optimization (AO) method to solve it. We prove that the obtained scheduling results are the same as the binary results from the AO method, which indicates that the primary rate requirements are always satisfied. Numerical results are provided to evaluate the performance of the proposed designs under different setups, as compared with benchmarks.

M. Hua, C. Li and L. Yang are with the School of Information Science and Engineering, Southeast University, Nanjing 210096, China (e-mail: {mhua, chunguoli, lxyang}@seu.edu.cn).

Q. Wu is with the State Key Laboratory of Internet of Things for Smart City and Department of Electrical and Computer Engineering, University of Macau, Macao 999078 China (email: qingqingwu@um.edu.mo).

C. Pan is with the School of Electronic Engineering and Computer Science, Queen Mary University of London, London E1 4NS, U.K. (e-mail: c.pan@qmul.ac.uk).

A. L. Swindlehurst is with the Center for Pervasive Communications and Computing, University of California at Irvine, Irvine, CA 92697 USA (e-mail: swindle@uci.edu).

## Index Terms

Intelligent reflecting surface (IRS), unmanned aerial vehicle (UAV), phase shift optimization, UAV trajectory optimization.

## I. INTRODUCTION

With the ever-growing sales of mobile devices and Internet of Things devices, current network architectures are becoming overwhelmed by growing data traffic demands [1]. Although numerous technologies such as millimeter wave (mmWave) communications, ultra-dense networks, and massive multiple-input multiple-output (MIMO) [2]–[4] have been proposed to address this problem, they are usually realized with very large energy consumption and high hardware cost due to the large number of RF chains required at the terminals. Recently, a new technology has come to the attention of the wireless research community, namely intelligent reflecting surfaces (IRS), due to its potential ability to reconfigure the radio propagation environment in a favorable way for transceiver optimization. An IRS is comprised of a manmade surface of electromagnetic material consisting of a large number of square metallic patches, each of which can be digitally controlled to induce different reflection amplitude, phase, and polarization responses on the incident signals [5], [6]. Since an IRS typically has numerous patch units (such as PIN-diodes), it can provide a significant passive beamforming gain without the need for RF chains, thus yielding a cost- and energy-efficient solution. For example, experiments conducted recently in [7] showed that for a large IRS consisting of 1720 reflecting elements, the total power consumption is only 0.280W. Therefore, IRS are a promising solution for improving the spectral and energy efficiency of wireless networks, and paving the way to the green networks of the future.

The new research paradigm of IRS-aided wireless communication has been extensively studied; e.g., see [5], [8], [9]. The authors of [5] provide an overview of the promising IRS technology for achieving smart and reconfigurable environments in future wireless networks. The authors of [8] discuss IRS in the general context of uniting information and electromagnetic theory in order to create smart radio environments, and report numerous promising directions for employing appropriate physics-based models of metasurfaces in wireless communications. Recently, there have been many contributions devoting efforts to integrating IRS into the current cellular networks. Joint active and passive beamforming design was investigated to either maximize the system throughput or minimize the BS transmit power in [10]–[12]. In particular, the authors in [10] studied the BS transmit power minimization problem by jointly optimizing the BS beamforming

matrix and IRS phase shift matrix while satisfying the users' minimum signal-to-interference-plus-noise ratio (SINR) requirement, and the results showed that for a single-user IRS-aided system, the received signal-to-noise ratio (SNR) increases quadratically with the number of reflecting elements. In addition, the applications of IRS are also appealing for numerous different system setups such as spectrum sharing [13], physical layer security [14], orthogonal multiple access [15], and simultaneous wireless information and power transfer [16], [17].

Unlike the above studies in which the IRS is used purely to assist the transmissions of the existing system, a new IRS functionality referred to as symbolic radio transmission has been proposed, where the information bits are carried by the on/off states of the IRS, while passive beamforming is achieved by adjusting the phase shift of each reflecting element [18], [19]. Specifically, a sensor is integrated into the IRS system, which for example collects environmental information such as temperature, humidity, illuminating light, etc., and sends it to a smart controller at the IRS via a wired link. Then, the controller transmits the collected information to the base station (BS) by adjusting the on/off state of the IRS. In fact, this idea has been tested experimentally in [20], where a motion-sensitive smart metasurface was integrated with a three-axis gyroscope on an aircraft to sense its direction of motion, allowing a smart controller to adaptively adjust the IRS phase shifts to maintain a beam pointed at a desired receiver. Each IRS reflecting element updated by the smart controller is able to induce an independent phase shift on the incident signal to change the signal propagation such that the desired and interfering signals can be added constructively or destructively to assist the communication system.

In this paper, we study an unmanned aerial vehicle (UAV)-assisted IRS symbiotic radio system, where the UAV is leveraged to assist the IRS data transmission. Specifically, we consider an urban environment, where there are multiple IRS available to sense environmental information. As shown in Fig. 1, the IRS sends its own data to the BS by controlling its on/off state, and the receiver side (BS) uses the difference in channel response caused by the on/off state to decode the IRS information. The IRS also simultaneously tunes each reflecting element to align the phase of the signal passing through the UAV-IRS-BS link with that of the UAV-BS link to achieve coherent signal combining at the BS, thereby enhancing the UAV communication performance. In addition, the UAVs flexible mobility can be exploited to create favorable channel conditions for the UAV-BS and UAV-IRS links. Our goal in this paper is to maximize the IRS data transmission by jointly optimizing the UAV trajectory, IRS phase shift matrix, and IRS scheduling, subject to a minimum data rate requirement for the UAV. We study two optimization objectives, one based

on fairness for the IRS and the other on the weighted sum rate (WSR) of the IRS. Then, we develop two novel algorithms to solve them. The main contributions of this paper are summarized as follows:

- We first take into account IRS fairness, and formulate a max-min optimization problem. The resultant problem is a mixed integer and non-convex problem, which is in general difficult to solve optimally. We show that the commonly used relaxation-based method cannot be applied to this problem since the UAV's rate requirement constraints may not be satisfied by the binary reconstruction operation for scheduling. To address this issue, a novel penalty-based algorithm is proposed. We first transform the binary constraints into a series of equivalent equality constraints, and then propose a two-layer algorithm to solve the problem. Numerical results show the effectiveness of this penalty-based algorithm.
- We then consider the IRS WSR optimization problem, which is also a mixed integer and non-convex problem. Although the penalty-based algorithm can be applied to solve this problem, it incurs a high computational load due to the update of the penalty coefficient in each outer layer iteration. To develop a low complexity algorithm, we propose a relaxation-based method. Specifically, we first relax the binary scheduling variables to continuous variables, and then we develop an alternating optimization algorithm to solve the relaxed non-convex optimization problem. We prove that the converged relaxation scheduling variables are binary, which means that no reconstruct strategy is needed, and thus the UAV rate constraints are automatically satisfied. Numerical results show the proposed relaxation-based method converges within only a few iterations.
- We conduct simulation results for the two proposed scenarios to illustrate their performance. For the first scenario, the results show that the average max-min rate of the IRS is highly related to the IRS phase shift matrix. In addition, the average max-min rate can be significantly improved by the optimized UAV trajectory. For the second scenario, we study the impact of weighting factors on the system performance, and find that the optimized UAV trajectory places it closest to IRS with a high weighting factor.

The rest of this paper is organized as follows: Section II introduces the system model and problem formulation. In Sections III and IV, we study the max-min and WSR optimization problems, respectively. Numerical results are provided in Section V, and the paper is concluded in Section VI.

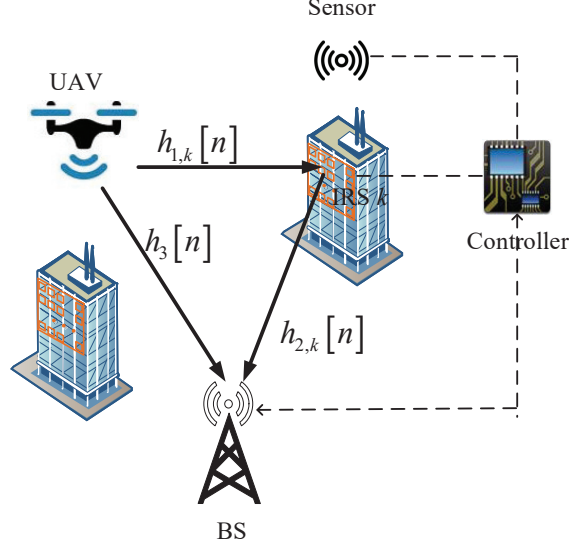


Fig. 1. UAV assisted IRS Symbiotic Radio System.

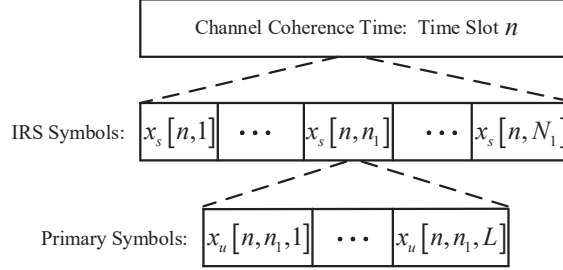


Fig. 2. Transmission frame for the IRS and primary transmission.

*Notations:* Boldface lower-case variables denote vectors. The notation  $\|\mathbf{x}\|$  represents the Euclidean norm of  $\mathbf{x}$ , the circularly symmetric complex Gaussian variable  $x$  with mean  $\mu$  and variance  $\sigma^2$  is denoted by  $x \sim \mathcal{CN}(\mu, \sigma^2)$ , statistical expectation is defined as  $\mathbb{E}\{\cdot\}$ , and  $\mathcal{O}(\cdot)$  denotes the big-O computational complexity notation.

## II. SYSTEM MODEL AND PROBLEM FORMULATION

### A. System Model

Consider a UAV-assisted IRS symbiotic radio system consisting of a single-antenna BS, a single-antenna UAV, and  $K$  IRSs as shown in Fig. 1, where the UAV acts to help the IRS transmit its own data to the BS. The BS and IRS are in fixed locations, and the UAV can freely adjust its heading as it moves. The horizontal coordinates of the BS and the  $k$ th IRS are respectively

denoted as  $\mathbf{q}_b = [q_b^x, q_b^y]^T$  and  $\mathbf{q}_{s,k} = [q_{s,k}^x, q_{s,k}^y]^T$ . In addition, the altitudes of the BS and the  $k$ th IRS are respectively denoted as  $H_b$  and  $H_s$ . We assume that the UAV flies in a periodic trajectory at a fixed altitude  $H_u$  and with a given period  $T$ . To make the problem tractable, the period  $T$  is equally divided into  $N$  time slots of duration  $\delta = T/N$ . As a result, the trajectory of the UAV can be approximated by the  $N$  two-dimensional sequences  $\mathbf{q}_u[n] = [q_u^x[n], q_u^y[n]]^T$ . Note that the duration  $\delta$  should be chosen to be sufficiently small to satisfy  $V_{\max}\delta \ll H_u$ , where  $V_{\max}$  denotes the maximum UAV speed, so that the UAV's location can be considered as approximately unchanged within each time slot. The UAV mobility constraints are given below:

$$\|\mathbf{q}_u[n] - \mathbf{q}_u[n-1]\| \leq V_{\max}\delta, \forall n, \quad (1)$$

$$\mathbf{q}_u[0] = \mathbf{q}_I, \mathbf{q}_u[N] = \mathbf{q}_F, \quad (2)$$

where  $\mathbf{q}_I$  and  $\mathbf{q}_F$  represent the UAV's initial and final location, respectively.

It is assumed that the IRS has  $M$  reflecting elements, and the reflection coefficient matrix of IRS  $k$  at time slot  $n$  is defined by the diagonal matrix  $\mathbf{\Theta}_k[n] = \text{diag}(e^{j\theta_{k,1}[n]}, \dots, e^{j\theta_{k,M}[n]})$ , where  $\theta_{k,m}[n]$  denotes the phase shift corresponding to the  $m$ th reflecting element of IRS  $k$  at time slot  $n$  [10], [16], [21]. Let  $\mathbf{h}_{1,k}[n] \in \mathbb{C}^{M \times 1}$ ,  $\mathbf{h}_{2,k}[n] \in \mathbb{C}^{M \times 1}$ , and  $h_3[n] \in \mathbb{C}^{1 \times 1}$  respectively denote the complex equivalent baseband channel vector between the UAV and the  $k$ th IRS, between the  $k$ th IRS and the BS, and between the UAV and the BS, at time slot  $n$ ,  $\forall k \in \mathcal{K}$ . To capture both the large-scale and small-scale fading, we model all channels as Rician [22]. Specifically, the channel coefficient between the UAV and IRS  $k$  at time slot  $n$  is given by [23]

$$\mathbf{h}_{1,k}[n] = \sqrt{\beta_{1,k}[n]} \left( \sqrt{\frac{K_1}{K_1 + 1}} \mathbf{h}_{1,k}^{\text{LoS}}[n] + \sqrt{\frac{1}{K_1 + 1}} \mathbf{h}_{1,k}^{\text{NLoS}}[n] \right), \quad (3)$$

where  $\beta_{1,k}[n]$  represents the large-scale fading channel coefficient,  $\mathbf{h}_{1,k}^{\text{LoS}}[n]$  and  $\mathbf{h}_{1,k}^{\text{NLoS}}[n]$  denote the deterministic LoS channel component and the small-scale fading component, respectively, and  $K_1$  is the Rician factor. The value of  $\beta_{1,k}[n]$  is related to the communication distance, and is given by

$$\beta_{1,k}[n] = \frac{\beta_0}{d_{1,k}^{\alpha_1}[n]} = \frac{\beta_0}{(\|\mathbf{q}_u[n] - \mathbf{q}_{s,k}\|^2 + (H_u - H_s)^2)^{\alpha_1/2}}, \quad (4)$$

where  $\beta_0$  denotes the channel power at the reference distance of 1 meter,  $d_{1,k}[n]$  is the distance between the UAV and IRS  $k$ , and  $\alpha_1$  denotes the path loss exponent. We assume that the IRS

employs a uniform linear array of reflecting elements<sup>1</sup>, and thus  $\mathbf{h}_{1,k}^{\text{LoS}}[n]$  is given by [23]

$$\mathbf{h}_{1,k}^{\text{LoS}}[n] = e^{-j\frac{2\pi d_{1,k}[n]}{\lambda}} \times \left[1, e^{-j\frac{2\pi d}{\lambda} \cos \phi_{1,k}[n]}, \dots, e^{-j\frac{2\pi(M-1)d}{\lambda} \cos \phi_{1,k}[n]} \right]^T, \quad (5)$$

where  $d$  denotes the IRS element spacing,  $\lambda$  denotes the carrier wavelength, and  $\cos \phi_{1,k}[n] = \frac{q_{s,k}^x - q_u^x[n]}{d_{1,k}[n]}$  is the cosine of the angle of arrival (AoA) [24], [25]. The elements of  $\mathbf{h}_{1,k}^{\text{NLoS}}[n]$  of the non-LoS component are assumed to be independent and identically distributed with zero mean and unit variance.

Similarly, the channel vector between IRS  $k$  and the BS at time slot  $n$  is expressed as

$$\mathbf{h}_{2,k}[n] = \sqrt{\beta_{2,k}} \left( \sqrt{\frac{K_2}{K_2 + 1}} \mathbf{h}_{2,k}^{\text{LoS}} + \sqrt{\frac{1}{K_2 + 1}} \mathbf{h}_{2,k}^{\text{NLoS}}[n] \right), \quad (6)$$

where  $\beta_{2,k} = \frac{\beta_0}{d_{2,k}^{\alpha_2}}$ ,  $d_{2,k} = \sqrt{\|\mathbf{q}_b - \mathbf{q}_{s,k}\|^2 + (H_b - H_s)^2}$ ,  $\alpha_2$  represents the path loss exponent, and  $K_2$  is the corresponding Rician factor. In addition,  $\mathbf{h}_{2,k}^{\text{LoS}} = e^{j\frac{2\pi d_{2,k}}{\lambda}} \left[1, e^{-j\frac{2\pi d}{\lambda} \cos \phi_{2,k}}, \dots, e^{-j\frac{2\pi(M-1)d}{\lambda} \cos \phi_{2,k}} \right]^T$ , where  $\cos \phi_{2,k} = \frac{q_b^x - q_{s,k}^x}{d_{2,k}}$  denotes the cosine of the angle of departure (AoD). The elements of  $\mathbf{h}_{2,k}^{\text{NLoS}}[n]$  are also assumed independent and identically distributed with zero mean and unit variance.

Finally, for the UAV-BS link at time slot  $n$  we have

$$h_3[n] = \sqrt{\beta_3[n]} \left( \sqrt{\frac{K_3}{K_3 + 1}} h_3^{\text{LoS}}[n] + \sqrt{\frac{1}{K_3 + 1}} h_3^{\text{NLoS}}[n] \right), \quad (7)$$

where  $\beta_3[n] = \frac{\beta_0}{d_3^{\alpha_3}[n]}$ ,  $d_3[n] = \sqrt{\|\mathbf{q}_u[n] - \mathbf{q}_b\|^2 + (H_b - H_u)^2}$ ,  $h_3^{\text{LoS}}[n] = e^{-j\frac{2\pi d_3[n]}{\lambda}}$ , path-loss exponent  $\alpha_3$ , and Rician factor  $K_3$ . As above, the elements of  $h_3^{\text{NLoS}}[n]$  are independent and identically distributed with zero mean and unit variance.

Typically, the symbol rate for the IRS transmission is much lower than that for the primary (UAV) transmission due to the limited computational and communication capabilities at the IRS. To describe it clearly, the frame structure for the IRS symbol, primary symbol, and channel coherence time is shown in Fig. 2. We assume that the duration of each UAV time slot equals the channel coherence time, i.e.,  $\delta = T_c$ . In the figure,  $x_{s,k}[n, n_1]$  represents the  $k$ th IRS symbol transmitted to the BS in the  $n_1$ th block of time slot  $n$ , and  $x_u[n, n_1, l]$  is the primary symbol transmitted from the UAV to the BS at the  $l$ th sub-block of block  $n_1$  within time slot  $n$ . Denote by  $T_s$  and  $T_u$  the durations of each IRS symbol and primary symbol, respectively. Without loss

<sup>1</sup>A uniform planar array at the IRS would provide steerability in elevation angle, but its analysis will be left as future work.

of generality, we assume that each IRS symbol covers  $L$  primary symbols, namely  $T_s = LT_u$ , where  $L$  is an integer, and  $L \gg 1$ . In addition, we assume  $\delta = T_c = N_1 T_s$ , where  $N_1$  is an integer, and  $N_1 \gg 1$ .

To facilitate the system design, we consider a widely used wake-up communication scheduling approach [26], [27], where the UAV can only communicate with at most one IRS<sup>2</sup> at any time slot  $n$ . Define the scheduling variable  $a_k[n]$ , where  $a_k[n] = 1$  indicates that IRS  $k$  is served by the UAV, and  $a_k[n] = 0$  otherwise. We then have the following scheduling constraints

$$\sum_{k=1}^K a_k[n] \leq 1, \forall n, \quad (8)$$

$$a_k[n] \in \{0, 1\}, \forall k, n. \quad (9)$$

If IRS  $k$  is communicating with the UAV in time slot  $n$ , the signal received by the BS at the  $l$ th sub-block of block  $n_1$  within time slot  $n$  is given by

$$\begin{aligned} y_{r,k}[n, n_1, l] = & \underbrace{\sqrt{P} (\mathbf{h}_{2,k}^H[n] \mathbf{\Theta}_k[n] \mathbf{h}_{1,k}[n, n_1] x_{s,k}[n, n_1])}_{\text{IRS-aided link}} x_u[n, n_1, l] + \underbrace{\sqrt{P} h_3[n] x_u[n, n_1, l]}_{\text{direct link}} \\ & + w[n, n_1, l], \end{aligned} \quad (10)$$

where  $P$  denotes the transmit power at the UAV,  $x_u[n, n_1, l] \sim \mathcal{CN}(0, 1)$ ,  $x_{s,k}[n, n_1] = \{0, 1\}$ , and  $w[n, n_1, l] \sim \mathcal{CN}(0, \sigma^2)$  denotes the noise at IRS  $k$  with power  $\sigma^2$ . Then, the achievable rate (bps/Hz) for the primary (UAV) system assisted by IRS  $k$  is given by

$$\begin{aligned} \bar{R}_{u,k}[n, n_1, l] = & \mathbb{E}_{x_{s,k}[n, n_1]} \left\{ \log_2 \left( 1 + \frac{P |h_3[n] + \mathbf{h}_{2,k}^H[n] \mathbf{\Theta}_k[n] \mathbf{h}_{1,k}[n, n_1]|^2}{\sigma^2} \right) \right\} \\ \stackrel{(a)}{=} & \rho \log_2 \left( 1 + \frac{P |h_3[n] + \mathbf{h}_{2,k}^H[n] \mathbf{\Theta}_k[n] \mathbf{h}_{1,k}[n, n_1]|^2}{\sigma^2} \right) + (1 - \rho) \log_2 \left( 1 + \frac{P |h_3[n]|^2}{\sigma^2} \right). \end{aligned} \quad (11)$$

where the second equality (a) holds since we assume that the probability for sending symbol “1” at IRS  $k$  is  $\rho$  ( $0 \leq \rho \leq 1$ ), and that for sending symbol “0” at IRS  $k$  is  $1 - \rho$ ,  $\forall k$ . It can be seen that the primary rate for each block of time slot  $n$  is the same. Thus, the achievable rate for the primary system assisted by IRS  $k$  at time slot  $n$  is given by  $\bar{R}_{u,k}[n] = \bar{R}_{u,k}[n, n_1, l]$ .

<sup>2</sup>Strictly speaking, the UAV directly communicates with the controller at IRS  $k$  rather than IRS itself. In the sequel, we will use the two terminologies interchangeably.



After decoding  $x_u[n, n_1, l]$ , successive interference cancellation (SIC) is applied at the BS to directly remove the direct link interference from the composite signals. Thus, we can obtain the intermediate signal as

$$\hat{y}_{r,k}[n, n_1, l] = \sqrt{P} (\mathbf{h}_{2,k}^H[n] \mathbf{\Theta}_k[n] \mathbf{h}_{1,k}[n] x_{s,k}[n, n_1]) x_u[n, n_1, l] + w[n, n_1, l]. \quad (12)$$

Note that since each IRS symbol covers  $L$  primary symbols, the IRS data transmission link can be treated as a multi-path component of the primary transmission. Thus, define  $\hat{\mathbf{y}}_{r,k}[n, n_1] = [\hat{y}_{r,k}[n, n_1, 1], \dots, \hat{y}_{r,k}[n, n_1, L]]^T$ , the reflecting rate for IRS  $k$  after applying the maximal ratio combining (MRC) technique can be obtained as [19], [28]

$$\bar{R}_{s,k}[n, n_1] = \log_2 \left( 1 + \frac{LP |\mathbf{h}_{2,k}^H[n] \mathbf{\Theta}_k[n] \mathbf{h}_{1,k}[n]|^2}{\sigma^2} \right). \quad (13)$$

We can see that the reflecting rate for each block of time slot  $n$  is the same. Thus, the achievable average rate for IRS  $k$  at time slot  $n$  is given by  $\bar{R}_{s,k}[n] = \bar{R}_{s,k}[n, n_1]$ .

Acquisition of instantaneous channel state information (CSI) for  $\{h_3[n], \mathbf{h}_{1,k}[n], \mathbf{h}_{2,k}[n]\}$  is difficult to obtain, especially the IRS-associated channels, i.e.,  $\{\mathbf{h}_{1,k}[n], \mathbf{h}_{2,k}[n]\}$ , due to their passive operation and the large number of IRS elements, which requires a prohibitive pilot training overhead as well as high signal processing complexity. Therefore, we propose an algorithm based on statistical CSI<sup>3</sup>, which is easier to implement compared with accurately tracking the instantaneous CSI at the IRS which varies much faster.

**Theorem 1:** The average achievable rate for the primary system, i.e.,  $\mathbb{E}\{\bar{R}_{u,k}[n]\}$ , is upper bounded by

$$\mathbb{E}\{\bar{R}_{u,k}[n]\} \leq \hat{R}_{u,k}[n] = (1 - \rho) \log_2 \left( 1 + \frac{P\beta_3[n]}{\sigma^2} \right) + \rho \log_2 \left( 1 + \frac{P \left( |x_{0,k}[n]|^2 + \frac{(K_1+K_2+1)M\beta_{1,k}[n]\beta_{2,k}}{(K_1+1)(K_2+1)} + \frac{\beta_3[n]}{K_3+1} \right)}{\sigma^2} \right), \quad (14)$$

where  $x_{0,k}[n] = \sqrt{\frac{K_3\beta_3[n]}{K_3+1}} h_3^{\text{LoS}}[n] + \sqrt{\frac{K_1K_2\beta_{1,k}[n]\beta_{2,k}}{(K_1+1)(K_2+1)}} (\mathbf{h}_{2,k}^{\text{LoS}}[n])^H \mathbf{\Phi}_k[n] \mathbf{h}_{1,k}^{\text{LoS}}[n]$ .

*Proof:* Please refer to Appendix A. ■

In Theorem 1, we can see that  $\hat{R}_{u,k}[n]$  is determined by the deterministic LoS channel components  $\{h_3^{\text{LoS}}[n], \mathbf{h}_{1,k}^{\text{LoS}}[n], \mathbf{h}_{2,k}^{\text{LoS}}[n]\}$ , the large-scale fading coefficients  $\{\beta_{1,k}[n], \beta_{2,k}, \beta_3[n]\}$ , and the IRS phase shift matrix  $\mathbf{\Phi}_k[n]$ .

<sup>3</sup>In this paper, statistical CSI refers to knowledge of the deterministic LoS components but only the distribution of the small-scale fading coefficients.

Similarly, we can obtain an upper bound of the reflecting rate for IRS  $k$  at time slot  $n$  as

$$E \{ \bar{R}_{s,k} [n] \} \leq \hat{R}_{s,k} [n] = \log_2 \left( 1 + \frac{P \left( |\bar{x}_{0,k} [n]|^2 + \frac{(K_1+K_2+1)M\beta_{1,k}[n]\beta_{2,k}}{(K_1+1)(K_2+1)} \right)}{\sigma^2} \right), \quad (15)$$

where  $\bar{x}_{0,k} [n] = \sqrt{\frac{K_1 K_2 \beta_{1,k}[n] \beta_{2,k}}{(K_1+1)(K_2+1)}} (\mathbf{h}_{2,k}^{\text{LoS}} [n])^H \mathbf{\Phi}_k [n] \mathbf{h}_{1,k}^{\text{LoS}} [n]$ . In the sequel, the upper bounds for the primary and reflecting rate are used as our utility functions. It is worth pointing out that the above approximations will be tight if the SNR is sufficiently high [29].

### B. Problem Formulation

For the first scenario, our goal is to maximize the minimum average rate among all IRS over all time slots by jointly optimizing the UAV trajectory, the IRS phase shift matrix, and the IRS scheduling. Accordingly, the problem can be formulated as

$$\max_{\theta_{k,m}[n], \mathbf{q}_u[n], a_k[n], R} R \quad (16a)$$

$$\text{s.t. } \frac{1}{N} \sum_{n=1}^N a_k [n] \hat{R}_{s,k} [n] \geq R, \forall k, \quad (16b)$$

$$\sum_{k=1}^K a_k [n] \hat{R}_{u,k} [n] \geq R_{\text{th}}, \forall n, \quad (16c)$$

$$0 \leq \theta_{k,m}[n] \leq 2\pi, \forall m, k, n, \quad (16d)$$

$$(1), (2), (8), (9). \quad (16e)$$

where  $R_{\text{th}}$  is the minimum rate requirement of the primary transmission system for any time slot  $n$ . The left hand side of (16b) denotes the achievable average rate of IRS  $k$  over all  $N$  time slots. Problem (16) is challenging to solve mainly due to the following two reasons. First, the optimization variables  $a_k[n]$  for communication scheduling are binary and thus (16b), (16c), and (9) involve integer constraints. Second, the IRS phase shift matrix, UAV trajectory, and IRS scheduling are intricately coupled in (16b) and (16c), which makes the problem non-convex. In general, there is no efficient method to optimally solve problem (16). One commonly used method would be to first relax the binary scheduling variables into continuous variables, then solve the relaxed non-convex problem, and finally convert the resulting continuous variables to binary [27], [30], [31]. However, this relaxation-based method cannot be applied to problem (16) due to the primary rate requirement (16c). More specifically, when converting the continuous-valued solutions for the  $a_k[n]$  obtained by the relaxed problem to binary, e.g., using the rounding

function [30], constraint (16c) will in general no longer be satisfied. To address this issue and obtain a high-quality suboptimal solution, we first transform the binary constraint (9) into a series of equivalent equality constraints. Then, a novel penalty-based algorithm is proposed to solve (16) whose solution for  $a_k[n]$  is guaranteed to be binary, and the constraints in (16c) are automatically satisfied.

For the second scenario, our goal is to maximize the weighted sum rate among all IRSs over all the time slots by jointly optimizing the UAV trajectory, IRS phase shift matrix, and IRS scheduling. Accordingly, the problem can be formulated as

$$\max_{\theta_{k,m}[n], \mathbf{q}_u[n], a_k[n]} \sum_{k=1}^K w_k \sum_{n=1}^N a_k[n] \hat{R}_{s,k}[n] \quad (17a)$$

$$\text{s.t.} \quad \sum_{k=1}^K a_k[n] \hat{R}_{u,k}[n] \geq R_{\text{th}}, \forall n, \quad (17b)$$

$$(1), (2), (8), (9), (16d), \quad (17c)$$

where  $w_k$  denotes the weighting factor for IRS  $k$ , with a higher value representing a higher priority over other IRS. Problem (17) is similar to problem (16), and thus can be also solved by the penalty-based method. However, this method requires a much higher computational complexity due to the outer layer iteration for updating the penalty coefficient. To address this issue, a relaxation-based method is proposed to solve problem (17). In Section IV, we prove that the relaxed solutions  $a_k[n]$  obtained by solving the proposed algorithm are binary, which means that no reconstruct strategy is needed, and thus the primary rate requirements in (17b) are always satisfied.

### III. PENALTY-BASED ALGORITHM FOR MAX-MIN PROBLEM

In this section, we propose a two-layer penalty-based algorithm to solve (16). The inner layer solves a penalized optimization problem by applying the AO method, while the outer layer updates the penalty coefficient, until convergence is achieved. Specifically, in the inner layer, the original problem (16) is decomposed into three subproblems: IRS phase shift matrix optimization, IRS scheduling optimization, and UAV trajectory optimization. However, even with this decomposition, the problem is still difficult to handle due to the non-convex cosine in both the objective function and constraints for the IRS phase shift and UAV trajectory subproblems. To address this issue, we first obtain a closed-form solution for the IRS phase shift matrix for a

given UAV trajectory and communication scheduling, and then substitute this expression into the original problem resulting in a joint IRS scheduling and UAV trajectory optimization problem. We first develop the following theorem:

**Theorem 2:** For any given UAV trajectory and IRS schedule, the optimal IRS phase shift matrix that maximizes the primary rate and IRS reflecting rate is given by

$$\theta_{k,m}^{\text{opt}}[n] = -\frac{2\pi d((\cos \phi_{2,k} - \cos \phi_{1,k}[n])(m-1) - (d_{1,k}[n] + d_{2,k}[n]) + d_3[n])}{\lambda}, \forall k, m. \quad (18)$$

*Proof:* Please refer to Appendix B. ■

From Appendix B, we can see that the maximizer of the terms  $|x_{0,k}[n]|^2$  and  $|\bar{x}_{0,k}[n]|^2$  are respectively given by

$$|x_{0,k}^*[n]|^2 = \frac{K_3\beta_3[n]}{K_3+1} + \frac{K_1K_2M^2\beta_{1,k}[n]\beta_{2,k}}{(K_1+1)(K_2+1)} + 2M\sqrt{\frac{K_1K_2K_3\beta_{1,k}[n]\beta_{2,k}\beta_3[n]}{(K_1+1)(K_2+1)(K_3+1)}}, \quad (19)$$

and

$$|\bar{x}_{0,k}^*[n]|^2 = \frac{K_1K_2M^2\beta_{1,k}[n]\beta_{2,k}}{(K_1+1)(K_2+1)}. \quad (20)$$

Substituting (19) and (20) in (14) and (15), respectively, we have

$$R_{u,k}[n] = (1-\rho)\log_2\left(1 + \frac{P\beta_3[n]}{\sigma^2}\right) + \rho\log_2\left(1 + \frac{P\left((c_{k,1}+c_{k,3})\beta_{1,k}[n] + c_{k,2}\sqrt{\beta_{1,k}[n]\beta_3[n]} + \beta_3[n]\right)}{\sigma^2}\right), \quad (21)$$

and

$$R_{s,k}[n] = \log_2\left(1 + \frac{LP(c_{k,1}+c_{k,3})\beta_{1,k}[n]}{\sigma^2}\right), \quad (22)$$

where  $c_{k,1} = \frac{K_1K_2M^2\beta_{2,k}}{(K_1+1)(K_2+1)}$ ,  $c_{k,2} = 2M\sqrt{\frac{K_1K_2K_3\beta_{2,k}}{(K_1+1)(K_2+1)(K_3+1)}}$ , and  $c_{k,3} = \frac{(1+K_1+K_2)M\beta_{2,k}}{(K_1+1)(K_2+1)}$ .

As a result, problem (16) is simplified as

$$\max_{\mathbf{q}_u[n], a_k[n], R} R \quad (23a)$$

$$\text{s.t. } \frac{1}{N} \sum_{n=1}^N a_k[n] \log_2 \left( 1 + \frac{LP(c_{k,1}+c_{k,3})\beta_{1,k}[n]}{\sigma^2} \right) \geq R, \forall k, \quad (23b)$$

$$\begin{aligned} & \sum_{k=1}^K a_k[n] \left( \rho \log_2 \left( 1 + \frac{P \left( (c_{k,1}+c_{k,3})\beta_{1,k}[n] + c_{k,2}\sqrt{\beta_{1,k}[n]\beta_3[n]} + \beta_3[n] \right)}{\sigma^2} \right) \right. \\ & \left. + (1-\rho) \log_2 \left( 1 + \frac{P\beta_3[n]}{\sigma^2} \right) \right) \geq R_{\text{th}}, \forall n, \end{aligned} \quad (23c)$$

$$(1), (2), (8), (9). \quad (23d)$$

It can be seen that (23) only involves three variables,  $\mathbf{q}_u[n]$ ,  $a_k[n]$ , and  $R$ , and the cosine function no longer appears, which thus make the problem easier to solve.

However, (23) is still an integer and non-convex problem. To tackle this difficulty, we first introduce slack variables  $\{\bar{a}_k[n]\}$  to transform the binary constraints into a series of equivalent equality constraints. Specifically, (9) can be rewritten as

$$a_k[n] (1 - \bar{a}_k[n]) = 0, \forall k, n, \quad (24)$$

and

$$a_k[n] = \bar{a}_k[n], \forall k, n. \quad (25)$$

From (24) and (25), we can readily derive that the  $a_k[n]$  that satisfies the above two constraints must be either 1 or 0, which confirms the equivalence of the transformation of (9) into the two constraints. We then use (24) and (25) in a penalty term that is added to the objective function of (23), yielding the following optimization problem

$$\min_{\mathbf{q}_u[n], a_k[n], R, \bar{a}_k[n]} -R + \frac{1}{2\eta} \sum_{k=1}^K \sum_{n=1}^N (|a_k[n] (1 - \bar{a}_k[n])|^2 + |a_k[n] - \bar{a}_k[n]|^2) \quad (26a)$$

$$\text{s.t. } (1), (2), (8), (23b), (23c) \quad (26b)$$

where  $\eta > 0$  is the penalty coefficient used to penalize the violation the equality constraints (24) and (25) [32]. While these equality constraints become satisfied as  $\eta \rightarrow 0$ , it is not effective to initially set  $\eta$  to be a very small value since in this case the objective will be dominated by the penalty terms, and the max-min term  $-R$  will be diminished. In contrast, initializing  $\eta$

with a larger value allows us to obtain a good starting point for the proposed algorithm. Then, by gradually decreasing the value of  $\eta$ , we can finally obtain a solution that satisfies (24) and (25) to within a predefined accuracy. Note that, for any given penalty coefficient  $\eta$ , problem (26) is still non-convex due to the non-convex constraints (23b) and (23c). We then apply the AO method to iteratively optimize the primary variables in different blocks [32]. Specifically, in the inner layer, problem (26) is divided into three subproblems in which  $\{\bar{a}_k[n]\}$ ,  $\{a_k[n]\}$ , and  $\{\mathbf{q}_u[n]\}$ , and are optimized iteratively as follows:

#### A. Inner layer iteration

1) Optimizing  $\bar{a}_k[n]$  for given  $a_k[n]$  and  $\mathbf{q}_u[n]$ . This subproblem can be expressed as

$$\min_{R, \bar{a}_k[n]} -R + \frac{1}{2\eta} \sum_{k=1}^K \sum_{n=1}^N (|a_k[n](1 - \bar{a}_k[n])|^2 + |a_k[n] - \bar{a}_k[n]|^2) \quad (27a)$$

$$\text{s.t. (23b).} \quad (27b)$$

We can see that only the auxiliary variable  $\bar{a}_k[n]$  is involved in the objective function. Therefore, setting the derivative of (27) with respect to  $\bar{a}_k[n]$  to zero, the solution can be obtained as

$$\bar{a}_k^{\text{opt}}[n] = \frac{a_k[n] + a_k^2[n]}{1 + a_k^2[n]}, \forall k, n. \quad (28)$$

2) Optimizing  $a_k[n]$  for given  $\bar{a}_k[n]$  and  $\mathbf{q}_u[n]$ . This subproblem is written as

$$\min_{a_k[n], R} -R + \frac{1}{2\eta} \sum_{k=1}^K \sum_{n=1}^N (|a_k[n](1 - \bar{a}_k[n])|^2 + |a_k[n] - \bar{a}_k[n]|^2) \quad (29a)$$

$$\text{s.t. (8), (23b), (23c).} \quad (29b)$$

It can be seen that (29) is convex with a quadratic objective function and linear inequality constraints, which can be numerically solved by standard convex optimization techniques, such as the interior-point method [33].

3) Optimizing  $\mathbf{q}_u[n]$  for given  $a_k[n]$  and  $\bar{a}_k[n]$ . Ignoring the constant terms that are irrelevant to the UAV trajectory, this subproblem is formulated as:

$$\max_{\mathbf{q}_u[n], R} R \quad (30a)$$

$$\text{s.t. (1), (2), (23b), (23c).} \quad (30b)$$

Note that (30) is neither concave or quasi-concave due to the non-convex constraints (23b) and (23c). In general, there is no efficient method to obtain the optimal solution. In the following, we adopt the successive convex optimization technique to solve (30).

To this end, we introduce additional slack variables  $\{z_{1,k}[n]\}$  and  $\{z_3[n]\}$ , and recast (30) as

$$\max_{\mathbf{q}_u[n], R, z_{1,k}[n], z_3[n]} R \quad (31a)$$

$$\text{s.t. } \frac{1}{N} \sum_{n=1}^N a_k[n] \log_2 \left( 1 + \frac{LP(c_{k,1}+c_{k,3}) z_{1,k}[n]}{\sigma^2} \right) \geq R, \forall k, \quad (31b)$$

$$\begin{aligned} & \sum_{k=1}^K a_k[n] \left( \rho \log_2 \left( 1 + \frac{P \left( (c_{k,1}+c_{k,3}) z_{1,k}[n] + c_{k,2} \sqrt{z_{1,k}[n] z_3[n]} + z_3[n] \right)}{\sigma^2} \right) \right. \\ & \left. + (1-\rho) \log_2 \left( 1 + \frac{P z_3[n]}{\sigma^2} \right) \right) \geq R_{\text{th}}, \forall n, \end{aligned} \quad (31c)$$

$$\beta_{1,k}[n] \geq z_{1,k}[n], \forall k, n, \quad (31d)$$

$$\beta_3[n] \geq z_3[n], \forall n, \quad (31e)$$

$$(1), (2). \quad (31f)$$

It can be shown that at the optimal solution to (31), we must have  $\beta_{1,k}[n] = z_{1,k}[n]$  and  $\beta_3[n] = z_3[n]$ ,  $\forall k, n$ , since otherwise we can always increase  $z_{1,k}[n]$  (or  $z_3[n]$ ) without decreasing the value of the objective. Therefore, problem (31) is equivalent to problem (30). With this reformulation, constraint (31b) is now concave with respect to  $z_{1,k}[n]$ , but with the new non-convex constraints (31d) and (31e). The key observation is that in (31d), although  $\beta_{1,k}[n]$  is not convex with respect to  $\mathbf{q}_u[n]$ , it is convex with respect to  $\|\mathbf{q}_u[n] - \mathbf{q}_{s,k}\|^2$ .

Recall that any convex function is globally lower-bounded by its first-order Taylor expansion at any feasible point [33]. Therefore, for any local point  $\|\mathbf{q}_u^r[n] - \mathbf{q}_{s,k}\|^2$  obtained at the  $r$ th iteration, we have

$$\begin{aligned} \beta_{1,k}[n] & \geq \frac{\beta_0}{\left( \|\mathbf{q}_u^r[n] - \mathbf{q}_{s,k}\|^2 + (H_u - H_s)^2 \right)^{\alpha_1/2}} - \frac{\alpha_1 \beta_0}{2 \left( \|\mathbf{q}_u^r[n] - \mathbf{q}_{s,k}\|^2 + (H_u - H_s)^2 \right)^{\frac{\alpha_1}{2} + 1}} \\ & \times \left( \|\mathbf{q}_u[n] - \mathbf{q}_{s,k}\|^2 - \|\mathbf{q}_u^r[n] - \mathbf{q}_{s,k}\|^2 \right) \triangleq \varphi^{lb}(\beta_{1,k}[n]). \end{aligned} \quad (32)$$

Define the new constraint as

$$\varphi^{lb}(\beta_{1,k}[n]) \geq z_{1,k}[n], \forall k, n, \quad (33)$$

which is convex since  $\varphi^{lb}(\beta_{1,k}[n])$  is a quadratic function with respect to  $\mathbf{q}_u[n]$ . Similarly, (31e) can be replaced by

$$\frac{\beta_0}{(\|\mathbf{q}_u^r[n] - \mathbf{q}_b\|^2 + (H_u - H_b)^2)^{\frac{\alpha_3}{2}}} - \frac{\alpha_3\beta_0}{2(\|\mathbf{q}_u^r[n] - \mathbf{q}_b\|^2 + (H_u - H_b)^2)^{\frac{\alpha_3}{2}+1}} \times (\|\mathbf{q}_u[n] - \mathbf{q}_b\|^2 - \|\mathbf{q}_u^r[n] - \mathbf{q}_b\|^2) \geq z_3[n], \forall n, \quad (34)$$

which is also a convex constraint.

In addition, to tackle the non-convexity of constraint (31c), we introduce variable  $z_{2,k}[n]$ , and reformulate (31c) as

$$\sum_{k=1}^K a_k[n] \left( \rho \log_2 \left( 1 + \frac{P((c_{k,1} + c_{k,3})z_{1,k}[n] + c_{k,2}z_{2,k}[n] + z_3[n])}{\sigma^2} \right) + (1 - \rho) \log_2 \left( 1 + \frac{Pz_3[n]}{\sigma^2} \right) \right) \geq R_{th}, \forall n, \quad (35)$$

with the additional constraint

$$z_{1,k}[n] \geq \frac{z_{2,k}^2[n]}{z_3[n]}, \forall k, n. \quad (36)$$

Both constraints (35) and (36) are convex since we can see that the left hand side of (35) is a log function, which is concave, and the right hand side of (36) is a quadratic-over-linear fractional function, which is convex. As a result, for any given local points  $\|\mathbf{q}_u^r[n] - \mathbf{q}_{s,k}\|^2$  and  $\|\mathbf{q}_u^r[n] - \mathbf{q}_b\|^2$ , we have the following optimization problem

$$\max_{\mathbf{q}_u[n], z_{1,k}[n], z_{2,k}[n], z_3[n], R} R \quad (37a)$$

$$\text{s.t. (1), (2), (31b), (33), (34), (35), (36).} \quad (37b)$$

Based on the previous discussions, the objective function and all of the constraints are convex. Thus, (37) is a convex optimization problem that can be efficiently solved by, for example, the interior point method [33].

### B. Outer layer iteration

In the outer layer, we gradually decrease the value of the penalty coefficient  $\eta$  as follows

$$\eta = c\eta, \quad (38)$$

where  $c$  ( $0 < c < 1$ ) is a scaling factor, where a larger value of  $c$  can achieve better performance but at the cost of more iterations in the outer layer.



---

**Algorithm 1** Proposed penalty-based algorithm for solving problem (23).

---

- 1: **Initialize**  $a_k^{r_1}[n]$ ,  $\|\mathbf{q}_u^{r_1}[n] - \mathbf{q}_{s,k}\|^2$ ,  $\eta$ ,  $r_1 = 0$ ,  $r_2 = 0$ ,  $\varepsilon_1$ ,  $\varepsilon_2$ ,  $r_{\max}$ .
  - 2: **Repeat: outer layer**
  - 3:   **Repeat: inner layer**
  - 4:     Update  $\bar{a}_k^{r_1}[n]$  based on (28).
  - 5:     Update  $a_k^{r_1}[n]$  by solving problem (29).
  - 6:     Update  $\mathbf{q}_u^{r_1}[n]$  by solving problem (37).
  - 7:      $r_1 \leftarrow r_1 + 1$ .
  - 8:   **Until** the fractional decrease of the objective value of (26) is below a threshold or the maximum number of iterations  $r_{\max}$  is reached.
  - 9:   Update penalty coefficient  $\eta^{r_2}$  based on (38).
  - 10:    $r_2 \leftarrow r_2 + 1$ , and  $r_1 \leftarrow 0$ .
  - 11: **Until** the constraint violation  $\xi$  is below a threshold  $\varepsilon_2$
- 

### C. Convergence Analysis and Computational Complexity

To show the converged solutions of the proposed penalty-based algorithm, the terminal criteria for the outer layer is given as follows;

$$\xi = \max \{ |a_k[n] (1 - \bar{a}_k[n])|, |a_k[n] - \bar{a}_k[n]|, \forall k, n \}, \quad (39)$$

where  $\xi$  is a predefined accuracy. The detailed procedure of the penalty-based algorithm is summarized in Algorithm 1. In the inner layer, with the given penalty coefficient, the objective function of (26) is non-increasing over each iteration after applying the AO method, and the objective of (26) is bounded due to the limited flying time  $T$  and transmit power  $P$ . As such, a stationary point can be achieved in the inner layer. In the outer layer, we gradually decrease the penalty coefficient so that the equality constraints (24) and (25) are ultimately satisfied. Based on the results in [34, Appendix B], this penalty-based framework is guaranteed to converge to a stationary point.

The complexity of Algorithm 1 can be quantified as follows. In the inner layer, the main complexity of Algorithm 1 comes from steps 5 and 6. In step 5, the complexity of computing  $a_k[n]$  using the interior point method is  $\mathcal{O}(KN + 2N + 1)^{3.5}$  [35], where  $KN + 2N + 1$  stands for the number of variables [36]. Similarly, in step 6, the complexity required to compute the UAV trajectory is  $\mathcal{O}(2KN + 3N + 1)^{3.5}$  [35], where  $2KN + 3N + 1$  denotes the number of variables.

Therefore, the total complexity of Algorithm 1 is  $\mathcal{O}(L_{\text{outer}}L_{\text{inner}}((KN + 2N + 1)^{3.5} + (2KN + 3N + 1)^{3.5}))$ , where  $L_{\text{inner}}$  and  $L_{\text{outer}}$  respectively denote the number of iterations required for reaching convergence in the inner layer and outer layer.

#### IV. RELAXATION-BASED ALGORITHM FOR WSR OPTIMIZATION

Based on Theorem 2, (21), and (22) in Section III, the WSR problem (17) can be written as

$$\max_{\mathbf{q}_u[n], a_k[n]} \sum_{k=1}^K w_k \sum_{n=1}^N a_k[n] \log_2 \left( 1 + \frac{LP(c_{k,1} + c_{k,3}) \beta_{1,k}[n]}{\sigma^2} \right) \quad (40a)$$

$$\begin{aligned} \text{s.t. } \sum_{k=1}^K a_k[n] & \left( \rho \log_2 \left( 1 + \frac{P((c_{k,1} + c_{k,3}) \beta_{1,k}[n] + c_{k,2} \sqrt{\beta_{1,k}[n] \beta_3[n] + \beta_3[n]})}{\sigma^2} \right) \right. \\ & \left. + (1 - \rho) \log_2 \left( 1 + \frac{P\beta_3[n]}{\sigma^2} \right) \right) \geq R_{\text{th}}, \forall n, \end{aligned} \quad (40b)$$

$$(1), (2), (8), (9). \quad (40c)$$

Note that problem (40) can be also solved by Algorithm 1, but doing so would incur high computational complexity. In the following, a low complexity algorithm based on the relaxation method is proposed. Specifically, we first relax the binary variable  $a_k[n]$  to a continuous variable, and rewrite constraint (9) as follows:

$$0 \leq a_k[n] \leq 1, \forall k, n. \quad (41)$$

We then decompose the relaxed problem into two separate subproblems, IRS scheduling and UAV trajectory optimization, and then alternately optimize each one.

##### A. IRS Scheduling Optimization

For any given UAV trajectory  $\mathbf{q}_u[n]$ , the IRS scheduling problem of (40) becomes

$$\max_{a_k[n]} \sum_{k=1}^K w_k \sum_{n=1}^N a_k[n] \log_2 \left( 1 + \frac{LP(c_{k,1} + c_{k,3}) \beta_{1,k}[n]}{\sigma^2} \right) \quad (42a)$$

$$\text{s.t. } (8), (40b), (41). \quad (42b)$$

Since both the objective function and constraints are linear with respect to  $a_k[n]$ , problem (42) is thus a linear optimization problem.

**Theorem 3:** The optimal solution  $a_k^{\text{opt}}[n]$  to problem (42) is binary, i.e.,  $a_k^{\text{opt}}[n] \in \{0, 1\}$ .

*Proof:* Please refer to Appendix C. ■

---

**Algorithm 2** Proposed relaxation-based algorithm for solving problem (40).

---

- 1: **Initialize**  $\|\mathbf{q}_u^r[n] - \mathbf{q}_{s,k}\|^2$ ,  $r = 0$ ,  $r_{\max}$ .
  - 2: Relax binary scheduling variables as continuous variables, and set  $a_k^r[n] = 1/K$ .
  - 3: **Repeat**
  - 4:     Solve problem (42) for given  $\{\mathbf{q}_u^r[n]\}$ , and denote the optimal solution as  $\{a_k^{r+1}[n]\}$ .
  - 5:     Solve problem (44) for given  $\{a_k^{r+1}[n]\}$ , and denote the optimal solution as  $\{\mathbf{q}_u^{r+1}[n]\}$ .
  - 6:     Update  $r \leftarrow r + 1$ .
  - 7: **Until** the fractional increase in the objective value of (40) is below a threshold or the maximum number of iterations  $r_{\max}$  is reached.
- 

Theorem 3 shows that even though the binary constraint in the IRS scheduling problem of (42) has been relaxed, the obtained solution by is still a binary result. As such, no reconstruction operation is needed. In addition, since (42) is a linear optimization problem, it has very low computational complexity [37].

### B. UAV Trajectory Optimization

For any given IRS schedule  $a_k[n]$ , the UAV trajectory optimization problem of (40) becomes

$$\max_{\mathbf{q}_u[n]} \sum_{k=1}^K w_k \sum_{n=1}^N a_k[n] \log_2 \left( 1 + \frac{LP(c_{k,1} + c_{k,3}) \beta_{1,k}[n]}{\sigma^2} \right) \quad (43a)$$

$$\text{s.t. (1), (2), (40b).} \quad (43b)$$

Using the previous analysis of the UAV trajectory optimization for problem (30) in Section III, by introducing the same slack variables  $\{z_{1,k}[n], z_{2,k}[n], z_3[n]\}$  and local points  $\|\mathbf{q}_u^r[n] - \mathbf{q}_{s,k}\|^2$  and  $\|\mathbf{q}_u^r[n] - \mathbf{q}_b\|^2$ , we can directly derive the following equivalent convex optimization problem

$$\max_{\mathbf{q}_u[n], z_{1,k}[n], z_{2,k}[n], z_3[n]} \sum_{k=1}^K w_k \sum_{n=1}^N a_k[n] \log_2 \left( 1 + \frac{LP(c_{k,1} + c_{k,3}) z_{1,k}[n]}{\sigma^2} \right) \quad (44a)$$

$$\text{s.t. (1), (2), (33), (34), (35), (36).} \quad (44b)$$

### C. Convergence Analysis and Computational Complexity

In the proposed AO algorithm, we solve the relaxed problem (40) by iteratively solving problems (42) and (44), where the solution obtained for one subproblem in each iteration is

used as the initial point for the other. The detailed procedure for solving (40) is summarized in Algorithm 2. The convergence of Algorithm 2 has been well studied in [32], and is omitted here for brevity.

We now analyze the complexity of Algorithm 2. In step 4, (42) is a linear optimization problem whose complexity is  $\mathcal{O}(KN)$  [37], where  $KN$  denotes the number of variables. In step 5, the complexity for solving (44) by the interior point method is  $\mathcal{O}(2KN + 3N)^{3.5}$  [35], where  $2KN + 3N$  denotes the number of variables. Therefore, the total complexity of Algorithm 2 is  $\mathcal{O}(L_{\text{iter}}(KN + (2KN + 3N)^{3.5}))$ , where  $L_{\text{iter}}$  stands for the number of iterations required to reach convergence.

## V. NUMERICAL RESULTS

In this section, we provide numerical results to verify the performance of the proposed algorithm for the UAV assisted IRS symbiotic radio transmission system. In the simulation, the channel gain is set to  $\beta_0 = -30$  dB [38], and the noise power at the IRS is set to  $\sigma^2 = -60$  dBm [39]. The UAV altitude is fixed at  $H_u = 30$  m with transmit power  $P = 20$  dBm and maximum speed  $V_{\text{max}} = 10$  m/s. The UAV's initial and final location are set to  $\mathbf{q}_I = \mathbf{q}_F = [15\text{m } 0]^T$ . The altitudes of the BS and IRS are both set to  $H_s = H_b = 10$  m. The duration of each time slot is  $\delta = 0.1$  s. The path loss exponents for the UAV-IRS link, IRS-BS link, and UAV-BS link are assumed to be the same 2.4. In addition, the Rician factors for the above links are set to be 10 dB. Unless otherwise specified, we set  $L = 10$ ,  $\rho = 0.5$ ,  $\lambda = 0.1$  m,  $\varepsilon_2 = 10^{-3}$ ,  $\varepsilon_2 = 10^{-10}$ ,  $\eta = 500$ ,  $c = 0.7$ .

### A. Max-Min Optimization

This subsection evaluates the performance of Algorithm 1 for the max-min problem (16). We consider 5 IRS, which are located at  $\mathbf{q}_{s,1} = [30 \text{ m}, 30 \text{ m}]^T$ ,  $\mathbf{q}_{s,2} = [-30 \text{ m}, 30 \text{ m}]^T$ ,  $\mathbf{q}_{s,3} = [-40 \text{ m}, 0]^T$ ,  $\mathbf{q}_{s,4} = [-30 \text{ m}, -30 \text{ m}]^T$ ,  $\mathbf{q}_{s,5} = [30 \text{ m}, -30 \text{ m}]^T$  in a horizontal plane. Fig. 3 shows the penalty violation  $\xi$  in (39) and the convergence behavior of Algorithm 1 under for different periods  $T$ . It can be seen from Fig. 3(a) that  $\xi$  converges very fast with the value decreasing to  $10^{-10}$  after 33 iterations for  $T = 20$  s. Even when  $T = 40$  s, the constraint is eventually satisfied within the predefined accuracy (i.e.,  $10^{-10}$ ) by 33 iterations, which indicates that the proposed penalty-based algorithm can effectively tackle the binary scheduling constraints. In addition, in Fig. 3(b), we plot the max-min rate versus the number of outer layer iterations.

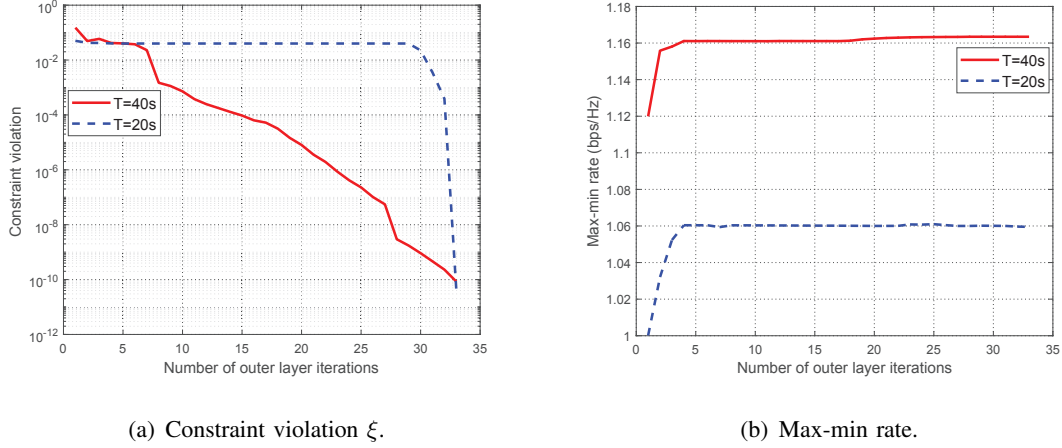


Fig. 3. Convergence behaviour of Algorithm 1.

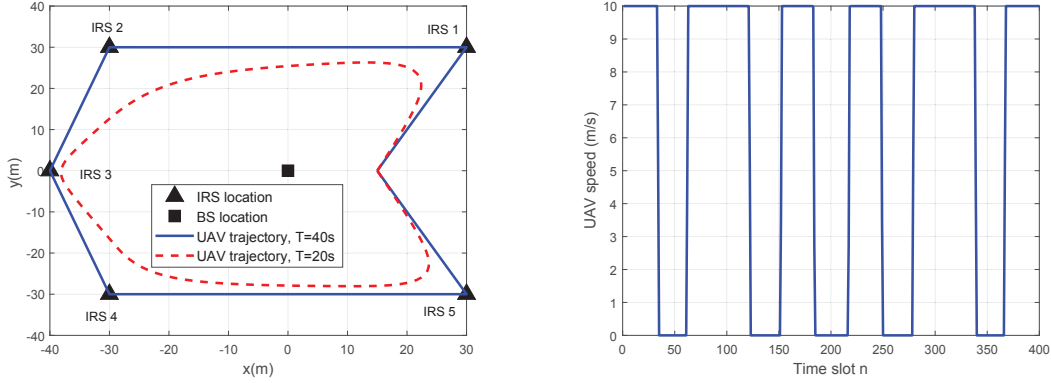
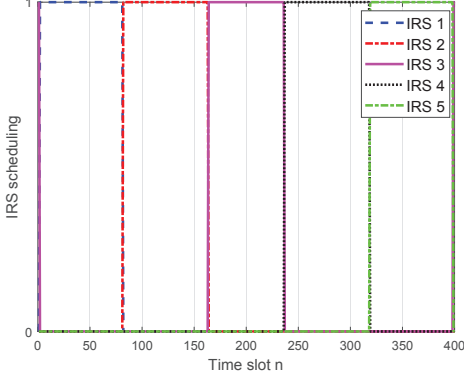
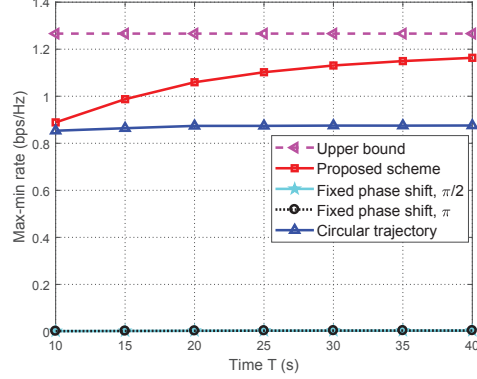


Fig. 4. Optimized UAV trajectories for different  $T$ .

Fig. 5. Optimized UAV speed for  $T = 40$  s.

We see that the max-min rate increases quickly with the number of outer layer iterations; for both the  $T = 20$  s and  $T = 40$  s cases, convergence to within a fraction of the final value is achieved only 4 iterations.

In Fig. 4, the optimized trajectories obtained by Algorithm 1 for  $T = 20$  s and  $T = 40$  s are plotted. As  $T$  increases, the UAV exploits its mobility to adaptively enlarge and adjust its trajectory to move closer to each IRS. When  $T$  becomes sufficiently large, i.e.,  $T = 40$  s, the UAV is able to sequentially visit all the IRS and stay stationary above each of them for a certain amount of time. This is expected since when the distance between the UAV and IRS is small, the length of the double channel fading propagation, i.e., the UAV-IRS-BS link, will be reduced, thus improving the IRS transmission rate. To see this more clearly, Fig. 5 plots the UAV speed

Fig. 6. Optimized IRS scheduling for  $T = 40s$ .Fig. 7. Max-min rate versus period  $T$ .

for the case when  $T = 40$  s. We see that the UAV flies either with maximum or zero speed, indicating that the UAV flies with maximum UAV speed to move closer to the IRS, and then remains stationary above it as soon as possible. Additionally, we observe in Fig. 6 that the IRS sequentially communicates with each UAV to experience better channel conditions, and the scheduling results are indeed binary, which demonstrates that the constraints in (24) and (25) are satisfied by the proposed Algorithm 1.

Fig.7 compares the max-min rate versus  $T$  achieved by the following schemes: 1) Proposed scheme in Algorithm 1; 2) Circular trajectory, where the UAV flies with a circle path of radius 15 m (corresponding to the distance from the BS to the UAV's initial/final location) and center  $[0, -0]^T$ ; 3) Fixed phase shifts, where the IRS phase shifts for all the elements is fixed at either  $\pi$  or  $\pi/2$ . For the fixed phase shift examples, the UAV trajectory is set to be the result obtained by the proposed scheme. It is first observed from Fig. 7 that our proposed algorithm substantially outperforms the other methods in terms of max-min rate. This is expected since an optimized UAV trajectory can establish better channel conditions for the IRS, which significantly increases IRS transmission rate. In addition, by adjusting the IRS phase shifts to align the cascaded AoA and AoD with the UAV-BS link, i.e., as shown in Theorem 2, the SNR of the UAV-IRS-BS link will be significantly increased. When  $T$  is sufficiently large, it can be assumed that the amount of time each IRS is served is equal. If the primary rate requirement is not difficult to achieve, such as for the case when the UAV hovers above the IRS, an upper bound for the max-min rate

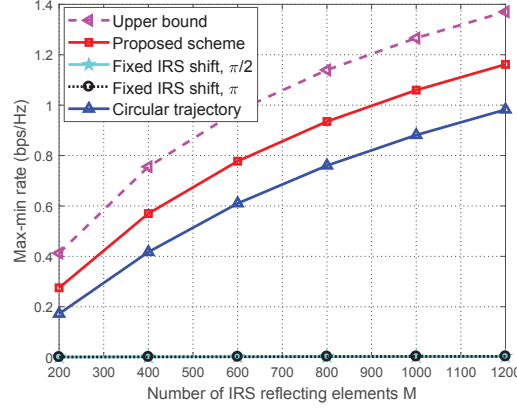


Fig. 8. Max-min rate versus the number of IRS reflecting elements.

can be obtained by solving the following problem

$$\max_{x_k \geq 0, R^{\text{upper}}} R^{\text{upper}} \quad (45a)$$

$$\text{s.t. } x_k \log_2 \left( 1 + \frac{LP(c_{k,1} + c_{k,2}) \beta_0}{\sigma^2 (H_u - H_s)^{\alpha_1}} \right) \geq R^{\text{upper}}, \forall k, \quad (45b)$$

$$\sum_{k=1}^K x_k = 1, \quad (45c)$$

where the term  $\log_2 \left( 1 + \frac{LP(c_{k,1} + c_{k,2}) \beta_0}{\sigma^2 (H_u - H_s)^{\alpha_1}} \right)$  represents the achievable rate for the IRS when the UAV is directly above IRS  $k$ , and  $x_k$  denotes the travel time ratio for IRS  $k$ . Problem (45) is a linear optimization problem, and thus can be easily solved by the interior point method.

In Fig. 8, the average max-min rate versus the number of IRS reflecting elements is studied. We see that the performance gain of the proposed scheme increases as the number of IRS reflecting elements increases, since more reflecting elements help achieve higher passive beamforming gain. In addition, the performance of the fixed IRS phase shift scheme is very poor, and the max-min rate nearly approaches zero due to the unaligned angles of the UAB-IRS-BS and UAV-BS links, which implies that the IRS phase shift must be carefully tuned.

### B. WSR Maximization

In this section, we study the WSR maximization problem. The initial setup for the WSR maximization simulations are the same as those used for evaluating the max-min approach discussed above. Unless otherwise specified, the weighting factors are set as  $\mathbf{w} = [1, 1, 1, 1, 1]^T$ .

To show the efficiency of Algorithm 2, its convergence behaviour for the two different periods  $T$  is plotted in Fig. 9. The average WSR increases quickly in the first few iterations, and in both cases converges within only 4 iterations.

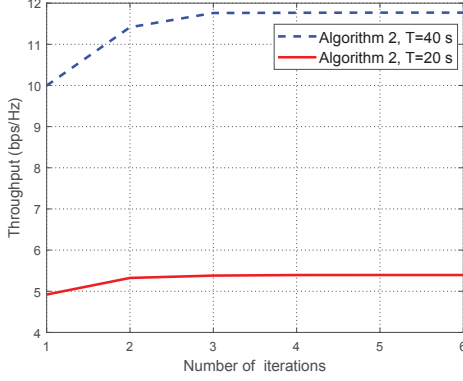


Fig. 9. Convergence behaviour of the proposed Algorithm 2 for different period.

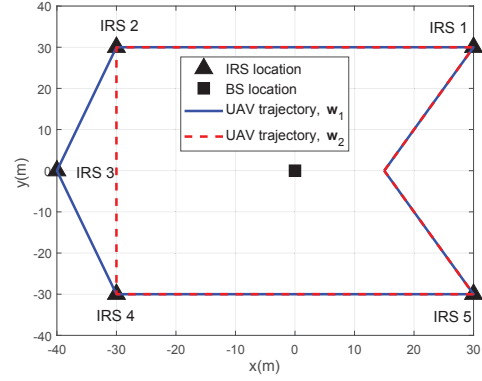


Fig. 10. Optimized UAV trajectory for different weighting factors.

In Fig. 10, the optimized UAV trajectories obtained by Algorithm 2 when  $T = 40$  s are studied for two different weighting factors, i.e.,  $\mathbf{w}_1 = [1, 1, 1, 1, 1]^T$  and  $\mathbf{w}_2 = [1, 1, 0.5, 1, 1]^T$ . We see that the UAV sequentially visits all IRS for the weighting factor  $\mathbf{w}_1$ , since the path loss between the UAV and IRS is significantly reduced when the UAV is nearby, thereby improving the system throughput. However, for weighting factor  $\mathbf{w}_2$ , the UAV only does a close fly-by of IRS 3 rather than hovering above it, since  $\mathbf{w}_2$  places a lower weight on IRS 3 and hence reduces its priority relative to the others. To see this more clearly, in Fig. 11 the UAV speed profile for the two weighting factors is plotted. Compared with  $\mathbf{w}_1$ , for  $\mathbf{w}_2$  the UAV spends less time hovering above IRS 3 for serving.

In Fig. 12, the IRS schedule for  $T = 40$  s is plotted. We see that for optimizing the WSR, the IRS are scheduled for different lengths of time, unlike the max-min case where each IRS is scheduled for essentially the same amount of time, time as shown in Fig. 6. As before, the IRS scheduling results are indeed binary, which verifies the effectiveness of Algorithm 2.

In Fig. 13, we study the throughput versus period  $T$  for our WSR algorithm compared with the same benchmarks as those considered for the max-min problem in Fig. 7. However, the calculation of the upper bound for the WSR problem is different from that for the max-min



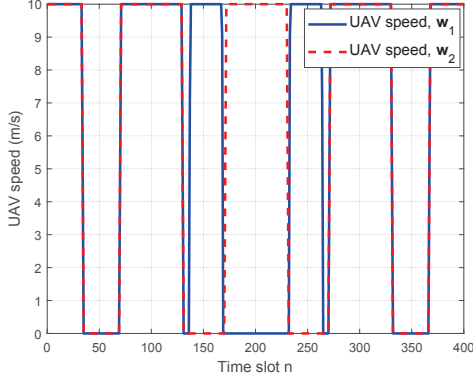
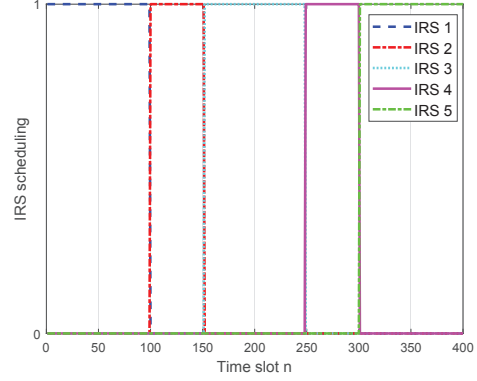
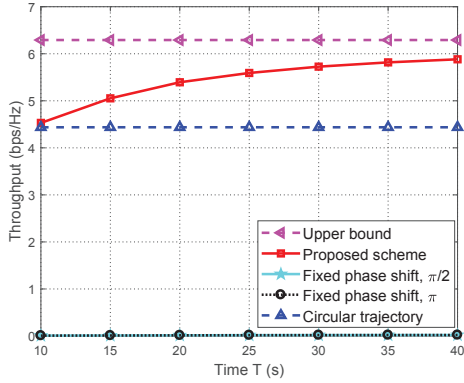
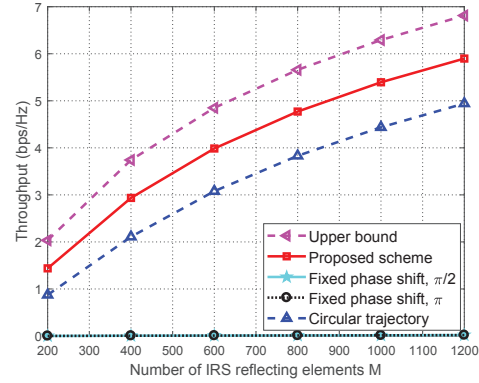
Fig. 11. UAV speed under  $T = 40$  s.Fig. 12. IRS scheduling under  $T = 40$  s.Fig. 13. Throughput versus period  $T$ .

Fig. 14. Throughput rate versus the number of IRS reflecting elements.

problem. The upper bound for WSR is given by the solution to

$$\max_{\forall k} \left\{ \log_2 \left( 1 + \frac{LP(c_{k,1} + c_{k,2})\beta_0}{\sigma^2(H_u - H_s)^{\alpha_1}} \right) \right\}. \quad (46)$$

Fig. 13 shows that the throughput for the circular trajectory is constant regardless of the period  $T$  due to the time-invariant air-to-ground channels. In contrast, the throughput achieved by the proposed scheme increases with  $T$ , which further demonstrates the benefits of leveraging the UAV mobility.

In Fig. 14, we study the throughput versus the number of IRS reflecting elements  $M$ . The performance gain of the proposed approach and the circular trajectory increases with  $M$ , since more reflecting elements help achieve higher passive beamforming gain. In addition, our proposed approach outperforms the circular trajectory by optimally leveraging the UAV mobility. Clearly,

the IRS has a significant impacts on the system performance, and the IRS phase shifts must be finely tuned in the system design.

## VI. CONCLUSION

In this paper, we studied a UAV-assisted IRS symbiotic radio system. We exploited the UAV mobility to maximize the data information transferred from several IRS to a given BS. We first considered fairness among the IRS, and developed a max-min optimization problem by jointly optimizing the UAV trajectory, IRS phase shifts, and IRS scheduling. To handle the resulting mixed integer non-convex problem, we transformed the binary constraints into an equivalent set of equality constraints, and proposed a penalty-based method to address the constraints. The effectiveness of this approach was justified by the numerical simulations. We then considered a weighted sum rate maximization problem, and we proposed a low-complexity relaxation-based method to solve it. We proved that the solution to the relaxed problem provides binary scheduling results, and hence no additional operation is needed to enforce this constraint. Simulation results demonstrated that the IRS transmission rate can be significantly improved by optimizing the UAV trajectory as well as the IRS phase shifts.

## APPENDIX A

### PROOF OF THEOREM 1

To show Theorem 1, we first define the function  $f(z) = \log_2(1+z)$ ,  $z \geq 0$ . It can be readily checked that  $f(z)$  is concave with respect to  $z$ . Thus, based on Jensen's inequality [33], we have  $\mathbb{E}\{f(z)\} \leq \log_2(1 + \mathbb{E}\{z\})$ . Therefore, the following inequality holds

$$\begin{aligned} \mathbb{E}\{\bar{R}_{u,k}[n]\} &\leq \rho \log_2 \left( 1 + \frac{P \mathbb{E}\left\{ \left| h_3[n] + \mathbf{h}_{2,k}^H[n] \mathbf{\Theta}_k[n] \mathbf{h}_{1,k}[n] \right|^2 \right\}}{\sigma^2} \right) + \\ &\quad (1 - \rho) \log_2 \left( 1 + \frac{P \mathbb{E}\{|h_3[n]|^2\}}{\sigma^2} \right). \end{aligned} \quad (47)$$

Since the small-scale fading channel coefficients  $h_3^{\text{NLoS}}[n]$ ,  $\mathbf{h}_{1,k}^{\text{NLoS}}[n]$ , and  $\mathbf{h}_{2,k}^{\text{NLoS}}[n]$  are independent of each other, we can obtain

$$\begin{aligned} \mathbb{E}\left\{ \left| h_3[n] + \mathbf{h}_{2,k}^H[n] \mathbf{\Theta}_k[n] \mathbf{h}_{1,k}[n] x_{s,k}[n] \right|^2 \right\} &= \\ |x_{0,k}[n]|^2 + \mathbb{E}\{|x_{1,k}[n]|^2\} + \mathbb{E}\{|x_{2,k}[n]|^2\} + \mathbb{E}\{|x_{3,k}[n]|^2\} + \mathbb{E}\{|x_{4,k}[n]|^2\}, \end{aligned} \quad (48)$$

where  $x_{0,k}[n] = \sqrt{\frac{K_3\beta_3[n]}{K_3+1}} h_3^{\text{LoS}}[n] + \sqrt{\frac{K_1K_2\beta_{1,k}[n]\beta_{2,k}}{(K_1+1)(K_2+1)}} (\mathbf{h}_{2,k}^{\text{LoS}}[n])^H \Phi_k[n] \mathbf{h}_{1,k}^{\text{LoS}}[n]$ ,  $x_{1,k}[n] = \sqrt{\frac{\beta_3[n]}{K_3+1}} h_3^{\text{NLoS}}[n]$ ,  $x_{2,k}[n] = \sqrt{\frac{K_1\beta_{1,k}[n]\beta_{2,k}}{(K_1+1)(K_2+1)}} (\mathbf{h}_{2,k}^{\text{NLoS}}[n])^H \Phi_k[n] \mathbf{h}_{1,k}^{\text{LoS}}[n]$ ,  $x_{3,k}[n] = \sqrt{\frac{K_2\beta_{1,k}[n]\beta_{2,k}}{(K_1+1)(K_2+1)}} (\mathbf{h}_{2,k}^{\text{LoS}}[n])^H \Phi_k[n] \mathbf{h}_{1,k}^{\text{NLoS}}[n]$ , and  $x_{4,k}[n] = \sqrt{\frac{\beta_{1,k}[n]\beta_{2,k}}{(K_1+1)(K_2+1)}} (\mathbf{h}_{2,k}^{\text{NLoS}}[n])^H \Phi_k[n] \mathbf{h}_{1,k}^{\text{NLoS}}[n]$ . We first calculate

$$\begin{aligned} \mathbb{E}\{|x_{2,k}[n]|^2\} &= \frac{K_1\beta_{1,k}[n]\beta_{2,k}}{(K_1+1)(K_2+1)} (\mathbf{h}_{1,k}^{\text{LoS}}[n])^H (\Phi_k[n])^H \mathbb{E}\left\{ \mathbf{h}_{2,k}^{\text{NLoS}}[n] (\mathbf{h}_{2,k}^{\text{NLoS}}[n])^H \right\} \Phi_k[n] \mathbf{h}_{1,k}^{\text{LoS}}[n] \\ &\stackrel{(a)}{=} \frac{K_1M\beta_{1,k}[n]\beta_{2,k}}{(K_1+1)(K_2+1)}, \end{aligned} \quad (49)$$

where (a) holds since  $\mathbb{E}\left\{ \mathbf{h}_{2,k}^{\text{NLoS}}[n] (\mathbf{h}_{2,k}^{\text{NLoS}}[n])^H \right\} = \mathbf{I}_M$ ,  $(\Phi_k[n])^H \Phi_k[n] = \mathbf{I}_M$ , and  $(\mathbf{h}_{1,k}^{\text{LoS}}[n])^H \mathbf{h}_{1,k}^{\text{LoS}}[n] = M$ . We can obtain the remaining terms as follows:

$$\mathbb{E}\{|x_{1,k}[n]|^2\} = \frac{\beta_3[n]}{K_3+1}, \mathbb{E}\{|x_{3,k}[n]|^2\} = \frac{K_2M\beta_{1,k}[n]\beta_{2,k}}{(K_1+1)(K_2+1)}, \mathbb{E}\{|x_{4,k}[n]|^2\} = \frac{M\beta_{1,k}[n]\beta_{2,k}}{(K_1+1)(K_2+1)}. \quad (50)$$

In addition, we have  $\mathbb{E}\{|h_3[n]|^2\} = \beta_3[n]$ . Combining all of the above results, we can directly arrive at (14).

## APPENDIX B

### PROOF OF THEOREM 2

Here we derive a closed-form solution for the IRS phase shifts that maximize the primary rate expression  $R_{u,k}[n]$  in (14). We have the following inequality

$$\begin{aligned} |x_{0,k}[n]| &= \left| \sqrt{\frac{K_3\beta_3[n]}{K_3+1}} h_3^{\text{LoS}}[n] + \sqrt{\frac{K_1K_2\beta_{1,k}[n]\beta_{2,k}}{(K_1+1)(K_2+1)}} (\mathbf{h}_{2,k}^{\text{LoS}}[n])^H \Phi_k[n] \mathbf{h}_{1,k}^{\text{LoS}}[n] \right| \\ &= \left| \sqrt{\frac{K_3\beta_3[n]}{K_3+1}} \exp\left(-j\frac{2\pi d_3[n]}{\lambda}\right) + \sqrt{\frac{K_1K_2\beta_{1,k}[n]\beta_{2,k}}{(K_1+1)(K_2+1)}} \exp\left(-j\frac{2\pi(d_{1,k}[n] + d_{2,k})}{\lambda}\right) \right. \\ &\quad \left. \sum_{m=1}^M \exp\left(j\left(\frac{2\pi d(\cos\phi_{2,k} - \cos\phi_{1,k}[n])(m-1)}{\lambda} + \theta_{k,m}[n]\right)\right) \right| \\ &\stackrel{(a)}{\leq} \left| \sqrt{\frac{K_3\beta_3[n]}{K_3+1}} \exp\left(-j\frac{2\pi d_3[n]}{\lambda}\right) \right| + \left| \sqrt{\frac{K_1K_2\beta_{1,k}[n]\beta_{2,k}}{(K_1+1)(K_2+1)}} \exp\left(-j\frac{2\pi(d_{1,k}[n] + d_{2,k})}{\lambda}\right) \right. \\ &\quad \left. \times \sum_{m=1}^M \exp\left(j\left(\frac{2\pi d(\cos\phi_{2,k} - \cos\phi_{1,k}[n])(m-1)}{\lambda} + \theta_{k,m}[n]\right)\right) \right|, \end{aligned} \quad (51)$$

where (a) is due to the triangle inequality, which holds with equality if and only if  $-j\frac{2\pi d_3[n]}{\lambda} = -j\frac{2\pi(d_{1,k}[n] + d_{2,k})}{\lambda} + j\frac{2\pi d(\cos\phi_{2,k} - \cos\phi_{1,k}[n])(m-1)}{\lambda} + \theta_{k,m}[n]$ ,  $\forall m$ . This indicates that the  $m$ th phase

shift at IRS  $k$  should be tuned such that the phase of the signal that passes through the UAV-IRS and IRS-BS links is aligned with that of the signal over the UAV-BS direct link to achieve coherent signal combining at the BS. Thus, we can obtain the closed-form IRS phase shift expression in (18). In addition, it can be easily checked that  $\theta_{k,m}^{\text{opt}}[n]$  in (18) is also the optimal solution that maximizes the IRS reflecting rate in (15). This completes the proof of Theorem 2.

## APPENDIX C

### PROOF OF THEOREM 3

It can be readily verified that problem (42) satisfies Slater's condition, and thus strong duality holds and its optimal solution can be obtained by solving its dual problem [33]. Specifically, we first introduce the dual variables  $\{\lambda[n] \geq 0\}$  associated with the primary rate constraints (40b), and derive the partial Lagrangian of problem (42) as follows

$$\begin{aligned} \mathcal{L}(a_k[n], \lambda[n]) &= \sum_{k=1}^K w_k \sum_{n=1}^N a_k[n] R_{s,k}[n] + \sum_{n=1}^N \lambda[n] \left( \sum_{k=1}^K a_k[n] R_{u,k}[n] - R_{\text{th}} \right) \\ &= \sum_{n=1}^N \left( \sum_{k=1}^K (w_k R_{s,k}[n] + \lambda[n] R_{u,k}[n]) a_k[n] - \lambda[n] R_{\text{th}} \right). \end{aligned} \quad (52)$$

The Lagrange dual function of (42) is defined as

$$g(\lambda[n]) = \max_{a_k[n]} \mathcal{L}(a_k[n], \lambda[n]) \quad (53a)$$

$$\text{s.t. (8), (41).} \quad (53b)$$

It can be seen that the dual function (53) can be divided into  $N$  subproblems that can be solved in parallel. The  $n'$ -th subproblem of (53) can be written as

$$\max_{a_k[n']} \sum_{k=1}^K (w_k R_{s,k}[n'] + \lambda[n'] R_{u,k}[n']) a_k[n'] - \lambda[n'] R_{\text{th}} \quad (54a)$$

$$\text{s.t. } 0 \leq a_k[n'] \leq 1, \forall k, \quad (54b)$$

$$\sum_{k=1}^K a_k[n'] \leq 1. \quad (54c)$$

Obviously, for any given  $\lambda[n] \geq 0$ , we have  $w_k R_{s,k}[n'] + \lambda[n'] R_{u,k}[n'] > 0$ . It can be easily derived that the optimal solution  $a_k^{\text{opt}}[n']$  that maximizes (54) is either  $a_{k'}^{\text{opt}}[n'] = 1$  or  $a_k^{\text{opt}}[n'] = 0$  for  $k \neq k'$ , where subscript  $k'$  corresponds to the index that maximizes  $w_k R_{s,k}[n'] + \lambda[n'] R_{u,k}[n']$  among all  $k \in \{1, \dots, K\}$ . This also holds for the case that there are more than two IRS that

have the same maximum value of  $w_k R_{s,k} [n'] + \lambda [n'] R_{u,k} [n']$  among all  $k \in \{1, \dots, K\}$ . This thus completes the proof of Theorem 3.

## REFERENCES

- [1] Q. Wu, G. Y. Li, W. Chen, D. W. K. Ng, and R. Schober, "An overview of sustainable green 5G networks," *IEEE Wireless Commun.*, vol. 24, no. 4, pp. 72–80, Aug. 2017.
- [2] A. L. Swindlehurst, E. Ayanoglu, P. Heydari, and F. Capolino, "Millimeter-wave massive MIMO: The next wireless revolution?" *IEEE Commun. Mag.*, vol. 52, no. 9, pp. 56–62, Sept. 2014.
- [3] M. Kamel, W. Hamouda, and A. Youssef, "Ultra-dense networks: A survey," *IEEE Commun. Surveys Tuts.*, vol. 18, no. 4, pp. 2522–2545, 4th Quat. 2016.
- [4] L. Lu, G. Y. Li, A. L. Swindlehurst, A. Ashikhmin, and R. Zhang, "An overview of massive MIMO: Benefits and challenges," *IEEE J. Sel. Top. Sign. Proces.*, vol. 8, no. 5, pp. 742–758, Oct. 2014.
- [5] Q. Wu and R. Zhang, "Towards smart and reconfigurable environment: Intelligent reflecting surface aided wireless network," *IEEE Commun. Mag.*, vol. 58, no. 1, pp. 106–112, Jan. 2020.
- [6] T. J. Cui, S. Liu, and L. Zhang, "Information metamaterials and metasurfaces," *J. Phys. Chem. C*, vol. 5, no. 15, pp. 3644–3668, 2017.
- [7] W. Tang, M. Z. Chen, X. Chen, J. Y. Dai, Y. Han, M. Di Renzo, Y. Zeng, S. Jin, Q. Cheng, and T. J. Cui, "Wireless communications with reconfigurable intelligent surface: Path loss modeling and experimental measurement," 2019. [Online]. Available: <https://arxiv.org/abs/1911.05326>
- [8] Q. Wu, S. Zhang, B. Zheng, C. You, and R. Zhang, "Intelligent reflecting surface aided wireless communications: A tutorial," 2020. [Online]. Available: <https://arxiv.org/abs/2007.02759v2>
- [9] M. D. Renzo, A. Zappone, M. Debbah, M. Alouini, C. Yuen, J. de Rosny, and S. A. Tretyakov, "Smart radio environments empowered by reconfigurable intelligent surfaces: How it works, state of research, and road ahead," 2020. [Online]. Available: <https://arxiv.org/abs/2004.09352>
- [10] Q. Wu and R. Zhang, "Intelligent reflecting surface enhanced wireless network via joint active and passive beamforming," *IEEE Trans. Wireless Commun.*, vol. 18, no. 11, pp. 5394–5409, Nov. 2019.
- [11] R. Liu, M. Li, Q. Liu, and A. L. Swindlehurst, "Joint symbol-level precoding and reflecting designs for RIS-enhanced MU-MISO systems," 2019. [Online]. Available: <https://arxiv.org/abs/1912.11767>
- [12] C. Pan, H. Ren, K. Wang, W. Xu, M. ElKashlan, A. Nallanathan, and L. Hanzo, "Multicell MIMO communications relying on intelligent reflecting surface," *IEEE Trans. Wireless Commun.*, early access, 2020.
- [13] X. Guan, Q. Wu, and R. Zhang, "Joint power control and passive beamforming in IRS-assisted spectrum sharing," *IEEE Commun. Lett.*, vol. 24, no. 7, pp. 1553–1557, 2020.
- [14] H. Yang, Z. Xiong, J. Zhao, D. Niyato, L. Xiao, and Q. Wu, "Deep reinforcement learning based intelligent reflecting surface for secure wireless communications," 2020. [Online]. Available: <https://arxiv.org/abs/2002.12271v2>
- [15] Y. Yang, B. Zheng, S. Zhang, and R. Zhang, "Intelligent reflecting surface meets OFDM: Protocol design and rate maximization," 2019. [Online]. Available: <https://arxiv.org/abs/1906.09956>
- [16] Q. Wu and R. Zhang, "Weighted sum power maximization for intelligent reflecting surface aided SWIPT," *IEEE Wireless Commun. Lett.*, Dec. 2019, DOI: 10.1109/LWC.2019.2961656.
- [17] C. Pan, H. Ren, K. Wang, M. ElKashlan, A. Nallanathan, J. Wang, and L. Hanzo, "Intelligent reflecting surface enhanced MIMO broadcasting for simultaneous wireless information and power transfer," *IEEE J. Sel. Areas Commun.*, early access, 2020.

- [18] W. Yan, X. Kuai, and X. Yuan, "Passive beamforming and information transfer via large intelligent surface," 2019. [Online]. Available: <https://arxiv.org/abs/1905.01491>
- [19] Q. Zhang, Y. Liang, and H. V. Poor, "Large intelligent surface/antennas (LISA) assisted symbiotic radio for IoT communications," 2020. [Online]. Available: <https://arxiv.org/abs/2002.00340v1>
- [20] Q. Ma, G. D. Bai, H. B. Jing, C. Yang, L. Li, and T. J. Cui, "Smart metasurface with self-adaptively reprogrammable functions," *Light-Science & Applications*, vol. 8, no. 1, pp. 1–12, 2019.
- [21] G. Zhou, C. Pan, H. Ren, K. Wang, and A. Nallanathan, "Intelligent reflecting surface aided multigroup multicast MISO communication systems," *IEEE Trans. Signal Process.*, early access, 2020, Doi = 10.1109/TSP.2020.2990098.
- [22] C. Zhan and Y. Zeng, "Aerial-ground cost tradeoff for multi-UAV-enabled data collection in wireless sensor networks," *IEEE Trans. Commun.*, vol. 68, no. 3, pp. 1937–1950, Mar. 2020.
- [23] D. Tse and P. Viswanath, *Fundamentals of Wireless Communication*. Cambridge, U.K.: Cambridge Univ. Press, 2005.
- [24] S. Li, B. Duo, X. Yuan, Y. Liang, and M. Di Renzo, "Reconfigurable intelligent surface assisted UAV communication: Joint trajectory design and passive beamforming," *IEEE Wireless Commun. Lett.*, vol. 9, no. 5, pp. 716–720, May 2020.
- [25] H. Long, M. Chen, Z. Yang, B. Wang, Z. Li, X. Yun, and M. Shikh-Bahaei, "Reflections in the sky: Joint trajectory and passive beamforming design for secure UAV networks with reconfigurable intelligent surface," 2020. [Online]. Available: <https://arxiv.org/abs/2005.10559>
- [26] M. Hua, Y. Wang, Q. Wu, H. Dai, Y. Huang, and L. Yang, "Energy-efficient cooperative secure transmission in multi-UAV-enabled wireless networks," *IEEE Trans. Veh. Technol.*, vol. 68, no. 8, pp. 7761–7775, Aug. 2019.
- [27] Q. Wu, Y. Zeng, and R. Zhang, "Joint trajectory and communication design for multi-UAV enabled wireless networks," *IEEE Trans. Wireless Commun.*, vol. 17, no. 3, pp. 2109–2121, Mar. 2018.
- [28] R. Long, Y. Liang, H. Guo, G. Yang, and R. Zhang, "Symbiotic radio: A new communication paradigm for passive internet of things," *IEEE Internet of Things J.*, vol. 7, no. 2, pp. 1350–1363, Feb. 2020.
- [29] Y. Han, W. Tang, S. Jin, C. Wen, and X. Ma, "Large intelligent surface-assisted wireless communication exploiting statistical CSI," *IEEE Trans. Veh. Technol.*, vol. 68, no. 8, pp. 8238–8242, Aug. 2019.
- [30] M. Hua, L. Yang, C. Pan, and A. Nallanathan, "Throughput maximization for full-duplex UAV aided small cell wireless systems," *IEEE Wireless Commun. Lett.*, vol. 9, no. 4, pp. 475–479, Apr. 2020.
- [31] M. Hua, Y. Wang, Z. Zhang, C. Li, Y. Huang, and L. Yang, "Power-efficient communication in UAV-aided wireless sensor networks," *IEEE Communications Letters*, vol. 22, no. 6, pp. 1264–1267, Jun. 2018.
- [32] D. P. Bertsekas, *Nonlinear Programming*. Athena Scientific, 1999.
- [33] S. Boyd and L. Vandenberghe, *Convex optimization*. Cambridge university press, 2004.
- [34] Y. Cai, Q. Shi, B. Champagne, and G. Y. Li, "Joint transceiver design for secure downlink communications over an amplify-and-forward MIMO relay," *IEEE Trans. Commun.*, vol. 65, no. 9, pp. 3691–3704, Sept. 2017.
- [35] G. Zhang, Q. Wu, M. Cui, and R. Zhang, "Securing UAV communications via joint trajectory and power control," *IEEE Trans. Wireless Commun.*, vol. 18, no. 2, pp. 1376–1389, Feb. 2019.
- [36] S. Boyd, *EE364b Convex Optimization*. [Online]. Available: <https://web.stanford.edu/class/ee364b/lectures.html>
- [37] J. Gondzio and T. Terlaky, "A computational view of interior point methods," *Advances in linear and integer programming. Oxford Lecture Series in Mathematics and its Applications*, vol. 4, pp. 103–144, 1996.
- [38] J. Xu, Y. Zeng, and R. Zhang, "UAV-enabled wireless power transfer: Trajectory design and energy optimization," *IEEE Trans. Wireless Commun.*, vol. 17, no. 8, pp. 5092–5106, Aug. 2018.
- [39] F. Zhou, Y. Wu, R. Q. Hu, and Y. Qian, "Computation rate maximization in UAV-enabled wireless-powered mobile-edge computing systems," *IEEE J. Sel. Areas Commun.*, vol. 36, no. 9, pp. 1927–1941, Sept. 2018.